UCRL 554
Cy. 2

UNIVERSITY OF CALIFORNIA

Radiation Laboratory

TWO-WEEK LOAN COPY

This is a Library Circulating Copy which may be borrowed for two weeks. For a personal retention copy, call Tech. Info. Division, Ext. 5545

BERKELEY, CALIFORNIA

DISCLAIMER

This document was prepared as an account of work sponsored by the United States Government. While this document is believed to contain correct information, neither the United States Government nor any agency thereof, nor the Regents of the University of California, nor any of their employees, makes any warranty, express or implied, or assumes any legal responsibility for the accuracy, completeness, or usefulness of any information, apparatus, product, or process disclosed, or represents that its use would not infringe privately owned rights. Reference herein to any specific commercial product, process, or service by its trade name, trademark, manufacturer, or otherwise, does not necessarily constitute or imply its endorsement, recommendation, or favoring by the United States Government or any agency thereof, or the Regents of the University of California. The views and opinions of authors expressed herein do not necessarily state or reflect those of the United States Government or any agency thereof or the Regents of the University of California.

COPY 2

UNCLASSIFIED

UCRL 554
Unclassified Distribution

UNIVERSITY OF CALIFORNIA

Radiation Laboratory

Contract No. W-7405-eng-48

THE PROTON-PROTON INTERACTION

R. S. Christian and H. P. Noyes

December 23, 1949

Berkeley, California

INSTALLATION	No. of Copies
Argonne National Laboratory	8
Armed Forces Special Weapons Project	1
Atomic Energy Commission, Washington	2
Battelle Memorial Institute	1
Brookhaven National Laboratory	8
Bureau of Medicine and Surgery	1
Bureau of Ships	1
Carbide & Carbon Chemicals Corp. (K-25)	4
Carbide & Carbon Chemicals Corp. (Y-12)	4
Chicago Operations Office	1
Cleveland Area Office	1
Columbia University (Dunning)	1
Columbia University (Failla)	1
Dow Chemical Company	1
General Electric Company, Richland	6
Hanford Operations Office	1
Idaho Operations Office	1
Iowa State College	2
Kansas City	1
Kellex Corporation	2
Knolls Atomic Power Laboratory	4
Los Alamos	3
Mallinckrodt Chemical Works	1
Massachusetts Institute of Technology (Gaudin)	1
Massachusetts Institute of Technology (Kaufmann)	1
Mound Laboratory	3
National Advisory Committee for Aeronautics	2
National Bureau of Standards	2
Naval Radiological Defense Laboratory	2
NEPA Project	2
New Brunswick Laboratory	1
New York Operations Office	5
North American Aviation, Inc.	1
Oak Ridge National Laboratory	8
Patent Advisor, Washington	1
Rand Corporation	1
Sandia Base	1
Sylvania Electric Products, Inc.	1
Technical Information Branch, ORE	15
U. S. Public Health Service	1
UCLA Medical Research Laboratory (Warren)	1
University of California Radiation Laboratory	5
University of Rochester	2
University of Washington	1
Western Reserve University (Friedell)	2
Westinghouse Electric Corp.	4
Total	119

Information Division
Radiation Laboratory
Univ. of California
Berkeley, California

THE PROTON-PROTON INTERACTION

R. S. Christian and H. P. Noyes

December 23, 1949

INTRODUCTION

In this report we shall attempt to fit the proton-proton scattering data at 32[1][2] and 350 Mev[3] by the use of static nuclear potentials. This description is phenomenological and as such may be considered a sequel to the report concerned with determining the n-p interaction from the scattering data at 40, 90,[4][5][6] and 280 Mev.[7]

The success that was obtained in the n-p system would seem to be sufficient grounds for expecting that p-p scattering would likewise be interpretable by means of static potentials. In fact we might be tempted to predict the p-p nuclear potential from our knowledge of the n-p potential as determined by the high energy scattering. This prediction could be made either on the hypothesis that the nuclear potential is charge independent (i.e, depends only upon whether the two particles are in a singlet or triplet spin state), or in terms of an attempt to explain the saturation of nuclear forces.

If we were to follow the first assumption (the so-called symmetry hypothesis) there would be no free parameters entering the p-p theory, since the results of the n-p experiments are quite definite. For both singlet and triplet states these experiments show that there are no (or very small) odd parity forces. Therefore on the basis of charge symmetry one might expect that the n-p and p-p scattering would be quite similar. This is in obvious disagreement with the experimental results as is seen in Figure 1.

In order to better understand the prediction of the charge symmetric theory we must consider in more detail the fundamental differences between n-p and p-p

scattering. Firstly, for 32 Mev protons the coulomb repulsion is dominant in the scattering at angles less than 20°. Between 20° and 40° or 50° the angular variation is governed by the nuclear-coulomb interference terms. The remaining region around 90° is virtually the same as for simple nuclear scattering. Secondly, the p-p system, being composed of identical particles obeying the exclusion principle, has fewer states than the n-p system. Specifically only even parity singlet states and odd parity triplet states can be present. Thus scattering occurs only in ^1S, ^3P, ^1D, ^3F,... states, and the charge symmetric theory predicts the virtual absence of triplet scattering. The n-p system, on the contrary, has scattering from both singlet and triplet even parity states so that a direct comparison must be justified. In order to learn what part of the complete n-p scattering is singlet scattering we must recall that in order to lead to the low total n-p cross section the singlet range must be greater than 2×10^{-13} cm. This gives an angular distribution for the singlet cross section that has an even higher ratio of $\frac{\sigma(180^\circ)}{\sigma(90^\circ)}$ than the complete scattering from both states, making a direct comparison of the relative angular variation of the complete n-p and p-p cross sections possible in the region from 50° to 90°. Thus the 32 Mev p-p results show that the charge symmetry hypothesis is untenable.

Alternatively we could attempt to predict the p-p scattering by directing our attention to the phenomenon of the saturation of nuclear forces. The n-p experiments rule out the possibility of n-p repulsive forces of anything like the magnitude required to explain saturation. The low energy experiments show that the singlet p-p forces are attractive. Thus the only remaining way for the p-p forces to lead to saturation would be the existence of strong repulsive forces in the triplet state. Since the triplet scattering amplitude is antisymmetric, the scattering from a central triplet potential is zero at 90°. Hence such repulsive forces would lead to an angular cross section rising even more rapidly on either

side of 90° than that predicted by the charge symmetric theory and are conclusively excluded by the data.

Thus both the hypothesis of the charge independence of nuclear forces and the possibility of strong repulsive forces in the triplet p-p state such as seem to be required for the saturation of nuclear forces are already disallowed by the p-p scattering at 32 Mev. The 350 Mev scattering is even more strikingly anomalous (cf. Figure 1). The experiments indicate a nearly spherically symmetric distribution over the range from 41° to 90° having an absolute magnitude that is twice the maximum possible for S wave scattering alone. Since the n-p scattering at 280 Mev was in good agreement with a non-relativistic potential model it is difficult to accept this as a relativistic effect. Again both charge symmetry and repulsive triplet forces would lead to scattering strongly peaked at 0° and 180° and an order of magnitude lower in value at 90° than the observed p-p cross section, and are conclusively disproved. This scattering is superficially similar to classical hard sphere scattering. However, since the wavelength of 350 Mev protons is only three or four times shorter than the range of the attractive region that must surround and include such a sphere in order to explain the low energy results, the sphere cannot be made large enough to give classical hard sphere scattering at this energy. This point is discussed in more detail below.

In spite of the suprising divergence of the observed p-p scattering from that which had been expected previous to the experiments, it has proved possible to reconcile all the existing data with the scattering predicted from a static nuclear potential. This model consists of a shallow singlet potential and a highly singular triplet tensor potential. The main body of this paper is concerned with justifying this model.

In view of the apparently fundamental differences between the expected and the observed p-p scattering, and the various complicating factors in the analysis of

the data, we have devoted the first part of this report to a more or less qualitative discussion of p-p scattering. In this section we will give typical results for various potential models but will not discuss which radial dependence is to be preferred. Rather we wish to emphasize the salient features in the analysis in order to furnish a basis for understanding the calculations which follow in Part 2.

PART 1. QUALITATIVE DISCUSSION

It has been shown by many authors that the experiments below 14 Mev are compatible with S wave scattering alone[8] and that these experiments have determined only the scattering length and effective range.[9] This indicates that no one of the radial forms usually assumed is to be preferred. It need hardly be emphasized that the low energy experiments give little information concerning the interactions in states of higher angular momentum (especially the P state) other than putting upper limits on the magnitudes of the interactions in these states.

The n-p experiments at 40 Mev[4][6] have shown that there is scattering in the D state and little scattering in the P state, and that the magnitudes of these interactions could be determined. It was therefore expected that since the range of forces for the p-p system is comparable, the scattering would likewise occur primarily in the S, P and D states.

It was observed immediately, as has been pointed out in the experimental papers,[1][2] that the data was in good agreement with that predicted by S wave scattering alone. This is in definite disagreement with the scattering predicted by the usual potential models. The reason is that the S state interaction completely specifies the entire singlet interaction, and in particular the effective range is so long that the D wave predicted at this energy is incompatible with the experimental results. (It would of course be possible to choose a potential that would give only S scattering at 32 Mev, but the effective range of such a potential

would then be much too short to fit the low energy region.)

If we consider in detail the predictions of the usual models we find that even for the most cut off potential (the square well) the D phase shift is already too large (0.77°), and as is to be expected the more long-tailed Yukawa potential has an even larger D phase shift (1.4°). The adverse effect of such D phase shifts on the angular distribution can be readily seen by reference to the second panel of Figure 2. The origin of this effect is destructive interference between S and D wave scattering in the region around 90°. This interference term is proportional to $\sin \delta_S \sin \delta_D \cos (\delta_S - \delta_D) P_2$. ($P_2(\cos \theta) = 3/2 \cos^2 \theta - 1/2$) The usual models predict positive values for δ_S and δ_D, so that this term has a minimum at 90° as is observed in the n-p scattering but not in the p-p case. (Figure 2 also demonstrates that the coulomb scattering has little effect in the region from 50° to 90° and hence cannot alter this conclusion.)

The central triplet scattering amplitude being antisymmetric leads to a cross section that is zero at 90°, and since there is no interference with the singlet state it can only add to the rise away from 90°. Therefore scattering in this state will increase the discrepancy between the predictions made from the central force model and the experiments. Alternatively we can see this directly from the fact that the P scattering is proportional to $\sin^2 \delta_P \cos^2 \theta$, showing that the $\cos^2 \theta$ term must have a positive coefficient. These effects are illustrated in the third panel of Figure 2.

In order to explain the 32 Mev data, we require a model that would predict essentially spherically symmetric scattering in the absence of the coulomb field. We have already seen that central force scattering predicted by monatonically decreasing potential models of the usual radial form is in qualitative disagreement with experiment. Conceivably a more complicated radial dependence, such as a repulsive lip on a square well, could lead to negligible D phase shifts at

32 Mev. Attempts to build such models have been unsuccessful because they have effective ranges too short to fit the low energy data. In view of the straightforward interpretation of the n-p scattering and the inherent difficulty of using such a model to fit the 350 Mev data, it did not appear profitable to pursue such models any further.

The remaining alternative, within the framework of the potential picture, is the possibility that the D wave is masked by the scattering from tensor forces in the triplet state. A favorable result is predicted by the use of the Born approximation to compute the scattering (cf. Figure 3). (The Born approximation is [illegible] for the P waves since the centrifugal barrier reduces the effect of the nuclear potential to a small perturbation.) The scattering computed this way is peaked at 90° and hence can add to the singlet cross section, which dips at 90°, to give an almost flat nuclear cross section. When the coulomb effects are included the resulting angular distribution is quite similar to S wave scattering (cf. Figure 4). Thus a proper choice of range and depth for the tensor potential can lead to agreement with the experiments. (An alternative way of understanding why the scattering can have a finite value at 90° even though it takes place in odd states is that the tensor force brings about a change in angular momentum, and tesseral harmonics other than the Legendre polynomials enter into the scattering amplitude. We can then see that the presence of $Y_1^1(\theta,\phi) = e^{i\phi} \sin\theta$ in addition to $Y_1^0(\theta,\phi) = \cos\theta$ leads to terms with a $\sin^2\theta$ symmetry which when added to the $\cos^2\theta$ symmetry terms in the singlet scattering could lead to a flat nuclear cross section.)

The 350 Mev data will first be analyzed independently of the 32 Mev data. The two models so derived will then be compared and reconciled. In order to further emphasize the anomalous nature of the high energy scattering, we note that if we assumed (arbitrarily) that there were no interactions in other than S states the predicted cross section would be spherically symmetric but ten or more times too

small. (Recall that even the maximum possible S wave cross section is only one-half the measured value.)

To analyze the situation in somewhat more detail we shall first consider the scattering that would result from the singlet state (since in this state the potential is completely specified by the assumption of a particular radial form). At 350 Mev the Born approximation is valid for central scattering and predicts the strong forward maximum illustrated in Figure 5. Alternatively we may view the problem in terms of a partial wave decomposition. Only the even Legendre polynomials comprise the scattering amplitude. The even polynomials are all 1 at 0° and 180° and alternate in sign at 90° (e.g., $P_0(90^\circ) = 1$, $P_2(90^\circ) = -.5$, $P_4(90^\circ) = .375$, . . .). Scattering by the usual monatonic potential models predicts that all phase shifts will have the same sign, so that there is constructive interference at 0° and 180° and destructive interference at 90°, giving a characteristic peaking of the angular distribution.

In order to obtain a flat cross section it would be necessary to require that phase shifts of even parity alternate in sign with increasing ℓ, resulting in a singlet cross section peaked at 90°. Then if this cross section were added to the central triplet cross section (which is always zero at 90°) a flat cross section would result. It does not appear possible, however, to find a singlet potential that will fit the scattering in the low energy region while at the same time predicting the required alternation in sign of the high energy phase shifts.

Before turning to the tensor models we will first consider the so-called hard sphere scattering which can have the required characteristic of giving phase shifts of alternating sign. At this wave-length of 0.5×10^{-13} cm it might appear superficially that a repulsive core in the central potential would give the desired result. However, it is found that when the effective range is fitted the repulsive core cannot extend more than 0.7×10^{-13} cm. Since the repulsive core is then not

much larger than the wave-length of the proton, scattering occurs predominantly from the surrounding attractive region (which is required in order to give agreement with the low energy data). Such a model results in scattering in the high energy region similar to that predicted by more usual forms.

Again we must appeal to the tensor force in order to obtain agreement with the experimental data. In fact, if we recall that at 32 Mev we needed to add a triplet cross section that was peaked around 90° in order to mask the minimum in the singlet scattering we see that the situation at 350 Mev is very similar. We can again use the tensor force to obtain agreement, for in Born approximation scattering depends only on the combination kR where k is the wave number and R the range of the potential. That is, to produce the same scattering at a higher energy we need only contract the range by a factor that is the square root of the energy ratio, and adjust the depth to give the desired absolute magnitude to the scattering.

We therefore have indications of a tensor potential at both 32 and 350 Mev, and need only show that the requirements for the two cases are compatible. As the energy changes different regions of the potential will play the more dominant role. For example, at 32 Mev the potential region at distances of the order of 3 to 4×10^{-13} cm is most important while at 350 Mev the potential region at distances of the order of 1×10^{-13} cm has become important. By adjusting the range and depth of a tensor potential of any given radial form the predictions may be made to fit the 32 Mev experimental data. However at 350 Mev the P wave protons are able to explore the potential in to considerably shorter distances and it is necessary to have a strong interaction in this region in order to explain the very high 350 Mev cross section. The tensor scattering calculated for a singular potential in Born approximation as illustrated in Figure 3 illustrates these remarks. From the foregoing curves we can also see that an appreciable fraction of the 32 Mev scattering must be explained in terms of tensor forces if we wish to obtain

agreement with the high energy data. These curves further show that the tensor potential would probably have little effect below 10 Mev as the scattering amounts to less than 1 percent of the total scattering.

PART 2. CALCULATIONS

A. Methods

The singlet scattering from a potential of given radial form depending on two parameters is completely specified by the scattering length and effective range, which are determined by the scattering below 10 Mev. The general method of determining these parameters for a given radial dependence is discussed in detail by Blatt and Jackson.(9) The S scattering due to the nuclear potential alone at higher energies was calculated by direct numerical integration of the radial wave equation giving the S phase shift. The true S phase shift (in the presence of the coulomb field) was then obtained by treating the coulomb field as a perturbation according to the method of Chew and Goldberger.(10) The corrections amounted to approximately one degree or less. The D phase shift was calculated in Born approximation considering only the nuclear forces. (This method was checked by numerical integration in the case of the Yukawa poential, corrected for the coulomb field as above. The results at 32 Mev: 1.33° for the Born approximation, 1.45° for the exact nuclear calculation, 1.40° with the coulomb correction were assumed to be a satisfactory check.) Higher waves than the D were found to be negligible at 32 Mev.

As was shown in Part 1, it was not necessary to calculate any odd parity phase shifts due to central forces, but the tensor scattering was required. This was calculated using the exact values of the complex phase shifts, δ_{ℓ}^{Jms}, which enter into the tensor scattering. The result was in good agreement with that predicted by the Born approximation. There is a slight tendency for the Born approximation to predict somewhat larger angular variations than are found in the

more exact calculations. This can readily be understood in terms of the higher approximations of the Born approximation for then the scattering amplitude entering into each successive iteration (or each successive collision) is less well collimated than that entering the previous iteration, due to the scattering that occurs. A further small difference between the exact and the Born calculations occurs in the absolute magnitude, a tensor force taken with a positive sign (i.e., same sign as for the deuteron) always has less scattering in the exact calculation while the tensor force taken with a negative sign always has more scattering. A comparison between the exact predictions using the two signs and with the result of the Born approximation is afforded by reference to Figures 6 and 7.

The phase shifts arising from the coupled states entering the exact calculations were carried out by iteration (in the manner described in reference 6) after they had been cast in the form of coupled integral equations. In the case of the uncoupled states any of the methods usually applicable to central scattering may be used. We found that the integral variational expression was sufficiently accurate when the proper component of the plane wave was used as a trial function.

From the relatively small differences shown in Figures 6 and 7, we decided it was unnecessary to carry out the exact calculations for the nuclear part of the scattering. This is particularly so because we are able to offset any difference in absolute magnitude by choosing a slightly altered tensor depth (which will be determined only very roughly anyway from the present data). One difficulty with using the Born approximation is that the interference term (cf. Appendix 1, for a derivation of this term) between the nuclear and coulomb scattering identically vanishes, while the exact calculations at 32 Mev show that the P wave component of the nuclear scattering interferes appreciably with the coulomb scattering. We had therefore to compute two uncoupled phase shifts, δ_1^{00} and δ_1^{1+}, and also iterate the coupled $^3P_2 + {}^3F_2$ state. The iteration process is rather tedious and

as the magnitudes of the phase shifts were small compared with the uncoupled phase shifts, we used the WKB approximation to obtain these phase shifts. We shall consider this approximation in more detail below: If the two independent solutions of the coupled equations have the asymptotic form

$$a_{\ell L} \sim a_{\ell L} \sin\left(kx - \frac{\ell\pi}{2} + \delta^J_{\ell L}\right),$$

where $L = \ell$ or $2J - 1$ depending upon which is the dominant state, then the nuclear phase shift may be easily shown to be given by

$$e^{2i\delta^{Jm_s}_{\ell}} = \frac{e^{i(\delta^J_{\ell\ell} - \delta^J_{LL})} - a^J_{\ell L} a^J_{L\ell} e^{i(\delta^J_{\ell L} - \delta^J_{L\ell})} + 2i\sqrt{\frac{(2L+1)}{(2\ell+1)}} \frac{\langle SLJm_s | SL0m_s\rangle}{\langle S\ell Jm_s | S\ell 0m_s\rangle} a^J_{\ell L} \sin(\delta^J_{\ell\ell} - \delta^J_{\ell L})}{e^{-i(\delta^J_{\ell\ell} + \delta^J_{LL})} - a^J_{\ell L} a^J_{L\ell} e^{-i(\delta^J_{\ell L} + \delta^J_{L\ell})}}$$

where now $L = 2J - 1$ only, and we have set $a^J_{\ell\ell} = a^J_{LL} = 1$. In the case of the $^3P_2 + {}^3F_2$ state we have found that the Born approximation yields all quantities in this expression with the exception of δ^2_{11}, with sufficient accuracy. This we have computed by using the "equivalent central potential" (cf. reference 6) in WKB approximation and then applying the Born approximation to this potential to obtain the phase shift. δ^2_{11} is then the sum of two terms one of which is identical with that predicted by the Born approximation applied directly to the coupled equations and the other is of the nature of a correction term, and has the value

$$\Delta^2_{11} = \frac{36.6}{25.10} \frac{1}{kR} \int_0^\infty \left[xV_t(x)\right]^2 g_1{}^2(kx)\, dx$$

where we have written the tensor potential,

$$S_{12}V_t\left(\frac{r}{R}\right) = \left[\frac{3(\vec{\sigma}_1 \cdot \vec{r})(\vec{\sigma}_2 \cdot \vec{r})}{r^2} - \vec{\sigma}_1 \cdot \vec{\sigma}_2\right] V_t(x)$$

and

$$g_\ell(kx) = \sqrt{\frac{\pi kx}{2}}\, J_{\ell+\frac{1}{2}}(kx)$$

This procedure applied to the exponential and Yukawa radial dependences yields the coefficients of the interference terms within a few percent the coefficients determined from an exact calculation.

For the 350 Mev scattering the coulomb scattering was neglected and the singlet scattering was computed in Born approximation.

B. Results

The singlet cross sections for the square, exponential, and Yukawa models are shown in Figure 8. In each case the range and depth have been chosen to agree with Blatt and Jackson's low energy analysis. (The range and depth of the Yukawa potential and square well were determined independently by Chew and Goldberger before the results of Blatt and Jackson were available to us and agree with their assigned limits of error.) These parameters, together with the S and D phase shifts at 20 and 32 Mev, are collected in Table 1. Clearly there are significant differences in the angular distributions predicted by the various models. However, the magnitude of the D phase shift is always large enough to yield a curve that has a characteristically different shape than the experimental results in the region from 50° to 90° and too low in absolute value at 90°. The principal reason for this is the presence of a P_2 coefficient in the nuclear scattering arising from the interference between the S and the D waves.

The addition of a central P wave does not change the cross section at 90° as can be seen in Figure 9 where we have indicated the effect of adding positive and negative P phase shifts to the scattering predicted by the Yukawa model (which comes closest to fitting the 90° point). Clearly these curves do not agree with the experimental results, primarily because the nuclear cross section adds in the region from 50° to 90° (where the coulomb interference can be neglected).

It is seen from Table I that the D phase shift increases as the potential

becomes more long tailed. Since the D phase shift is too large even for the square potential we are forced to turn to more complicated radial forms, if we wish to account for the 32 Mev scattering by central interactions alone. Such a potential might be expected to be repulsive at long distances and attractive at short distances. Accordingly some attempts were made to annul the D wave by adding a repulsive lip to the square well. They met with little success, and having regard to the inherent difficulties implicit in such an approach when applied to attempt an explanation of the 350 Mev results, this approach was abandoned.

As discussed in Part 1, the effect of adding tensor force in the purely nuclear scattering is to produce a more nearly spherically symmetric angular distribution. The depth of the tensor potential and hence the amplitude of the scattering may be considered arbitrary, and must eventually be chosen to give agreement with the experimental data. In Figure 10 we have shown the result of adding the tensor scattering to the singlet state scattering. Clearly, if the same radial dependence is assumed to hold for both singlet and triplet states, approximate agreement may be obtained for the exponential potential with depth $V_t = \pm 50$ Mev. If we drop the restriction that the singlet and triplet potentials have the same radial dependence, it is clear that we can obtain better agreement, especially with the photographic data, by using the combination of square well for the singlet potential and Yukawa for the triplet (cf. Figure 11). (This combination utilizes a square well with the constants previously found for the singlet state and a tensor Yukawa well of range 1.25×10^{-13} cm and $V_t = \pm 26$ Mev.)

As was remarked in Part 1 tensor scattering at 32 Mev is only able to explore the tail of the potential, and consequently there is little uniqueness to the radial form which can be established from the 32 Mev data. To illustrate this we may consider the Born approximation. In this approximation the triplet differential

cross section (considering only the nuclear part) is proportional to

$$\sigma(\theta) \sim \left[C^2(\theta) + C^2(\pi - \theta) + C(\theta)\, C(\pi - \theta)\right]$$

where

$$C(\theta) = \frac{M}{\hbar^2 K} \int_0^\infty V_t \left(\frac{r}{R}\right) g_2\,(Kr)\, r dr \quad , \quad K = 2k \sin\frac{\theta}{2}$$

Plots proportional to $C(\theta)$ are shown in Figure 12 as a function of $\alpha(2kR \sin\frac{\theta}{2})$ where α has been adjusted such that each model predicts almost the same scattering at 32 Mev. (Recall that the Yukawa potential with $R = 1.25 \times 10^{-13}$ cm gave a good fit to the data when combined with a shallow singlet potential.) From these plots we find that the following ranges are practically equivalent with respect to the 32 Mev scattering: $R = 3.8 \times 10^{-13}$ cm (square), $R = 1.0 \times 10^{-13}$ cm (exponential), $R = 1.25 \times 10^{-13}$ cm (Yukawa), $R = 2.0 \times 10^{-13}$ cm^2 $\left(\exp(-r/R)/(r/R)^2\right)$.

In the plots of $C(\theta)$ we have chosen the scale of the abscissa such that $\alpha(2kR \sin\frac{\theta}{2}) = 1$ for $\theta = 90^\circ$ with a k corresponding to 32 Mev. For other angles we move up and down the abscissa according to $\sin\frac{\theta}{2}$ (e.g., to obtain the value for $C(180^\circ)$ at 32 Mev read the ordinate for an abscissa $\sqrt{2}$). The 90° point at other energies can be readily located as it is given at an abscissa which is the square root of the ratio of that energy to 32 Mev. Thus to obtain the value of $C(90^\circ)$ at 350 Mev read the ordinate at an abscissa of $\sqrt{\frac{350}{32}} = 3.30$.

As the energy increases a large difference in scattering occurs between the various models. The more shallow potentials give less scattering relative to that at 32 Mev. From the predictions of the various models for the singlet state it seems reasonable to allow approximately one-third of the nuclear scattering at 32 Mev to be of tensor origin. This gives a tensor cross section at 32 Mev which is comparable to the 350 Mev cross section in magnitude. We therefore see that the Yukawa and other even less concentrated (i.e., shallower) potentials do not predict a sufficiently high cross section at 350 Mev. It is therefore necessary to use the singular potential $\frac{e^{-r/R}}{\left(\frac{r}{R}\right)^2}$. The results for the complete cross section

at 350 Mev are compared in Figure 13. In order to indicate the essential features of the singular model, we again examine the curves in Figure 12. Clearly a square well of range 4×10^{-13} cm gives scattering of the correct form to fit the 32 Mev data, while a square well of range 1×10^{-13} cm gives 350 Mev scattering approximating to that predicted by the singular model. Thus by combining the shallow long range square well with a deep short range square well (which will not be explored by 32 Mev P wave protons) scattering approximating to that predicted by the singular model can be obtained.

C. Summary of Results

We have shown that the 32 Mev data can be fitted by means of two combinations of central and tensor force. These are: 1. The radial dependence is chosen the same for the central and tensor potential. The best fit is then with an exponential radial dependence of range 0.7×10^{-13} cm and with a tensor depth of $\pm$ 50 Mev. This model fits the counter data better than the photographic data. 2. The radial dependence is singular for the tensor potential and shallow and cut off for the central potential. The best fit is with a singlet square well of range 2.6×10^{-13} cm and with either a $V_t \exp(-r/R)/(r/R)$ radial dependence (with $R = 1.3 \times 10^{-13}$ cm and $V_t = \pm$ 26 Mev) or with a more singular potential $V_t \exp(-r/R)/(r/R)^2$ with $R = 2.0 \times 10^{-13}$ cm and $V_t = \pm$ 22 Mev. These combinations give better fits to the photographic data.

To fit the 350 Mev data we have shown that a very singular tensor force must be used, such as the $\exp(-r/R)/(r/R)^2$. The essential feature is that there must be a strong interaction in regions less than 0.5×10^{-13} cm.

The best fit of the combined data is therefore obtained by using the singular potential so adjusted that approximately one-third of the nuclear scattering at 32 Mev is accountable to tensor scattering.

It is clear that the present data are not sufficiently extensive to permit very precise specification of the radial forms; however, in the foregoing summary we have tried to emphasize the salient features of each model.

CONCLUSIONS

We have shown that it is possible to fit all the present p-p data by means of a shallow central potential for the singlet states and a singular tensor potential for the triplet states.

Quite apart from the potential models assumed, however, even the most casual comparison of the p-p data at 32 Mev with the n-p data at 40 Mev and, especially a comparison of the 340 Mev p-p data with the 280 Mev n-p data shows that nuclear scattering is charge dependent. In particular, there is definite evidence in the n-p scattering data that large tensor scattering does not occur in the odd parity states.

It is possible that the radial dependences found necessary for p-p scattering would be acceptable for the n-p scattering even though the exchange behavior is different. A definite statement regarding this must await detailed calculations, however.

Finally we must take notice of the fact that no large repulsive forces have shown up in either the n-p or the p-p system of sufficient magnitude to account for nuclear saturation if saturation is to be predicted from two body forces. In both cases they would have been very easily detected, independent of the potential model assumed.

ACKNOWLEDGMENTS

This analysis was originally started by G. F. Chew and M. L. Goldberger, to whom the analysis of the low energy data to obtain the singlet potential parameters and the original demonstration that the observed 32 Mev scattering is incompatible with central force models is due. We are indebted to J. M. Blatt and J. D. Jackson for receipt of their forthcoming paper on the analysis of the low energy proton-proton scattering prior to publication. We owe more than can be stated to the inspiration and guidance of Professor Robert Serber throughout this research.

The work described in this paper was performed under the auspices of the Atomic Energy Commission.

Information Division
scb/12-29-49

APPENDIX I

The triplet cross section is given by

$$\frac{d\sigma}{d\Omega} = \frac{1}{3k^2} \sum_{m_s} \left(|R|^2 + RN_o^* + N_oR^* + \sum_{\mu} N_\mu^* N_\mu \right) \tag{1A}$$

where

$$R = \frac{\alpha}{2i}\left(\frac{e^{-i\alpha \ln \sin^2\frac{\theta}{2}}}{\sin^2 \frac{\theta}{2}} - \frac{e^{-i\alpha \ln \cos^2 \frac{\theta}{2}}}{\cos^2 \frac{\theta}{2}} \right)$$

$$N_\mu = \sum_{J,\ell} \sqrt{4\pi(2\ell+1)}\; e^{2i(\sigma_\ell - \sigma_0)} \langle S\ell J m_s | S\ell 0 m_s \rangle \langle S\ell J m_s - \mu | S\ell \mu m_s - \mu \rangle \left(e^{2i\delta_\ell^{Jm_s}} - 1 \right) \bar{Y}_\ell^\mu(\theta,\phi)$$

$$\alpha = e^2/kv$$

$$\sigma_\ell - \sigma_0 = \tan^{-1}\frac{\alpha}{\ell} + \tan^{-1}\frac{\alpha}{\ell-1} + \ldots + \tan^{-1}\alpha$$

$\bar{Y}_\ell^\mu(\theta,\phi)$ are the normalized tesseral harmonics and $\delta_\ell^{Jm_s}$ are the customary (complex) phase shifts that occur in tensor scattering (defined here in the presence of the coulomb field).

In Equation (1A) the term involving $|R|^2$ is just the usual triplet coulomb scattering and the terms $\sum_\mu N_\mu^* N_\mu$ are the usual nuclear scattering. The remaining terms represent the interference between nuclear and coulomb scattering.

In our calculations of the tensor scattering the coulomb modification of the nuclear phase shift was neglected as the expected order of magnitude of this modification was very small compared to the P phase shifts. Further the nuclear-coulomb interference terms were calculated only for the P wave part of the nuclear scattering. These terms can then be written

$$\frac{9P_1(\cos\theta)}{2k^2}\left[\frac{\sin\alpha_1}{S^2} - \frac{\sin\beta_1}{C^2}\right]\left(\frac{1}{9}\sin^2\delta_1^{00} + \frac{1}{3}\sin^2\delta_1^{1\pm} - \frac{1}{6}A_1^{2\pm} - \frac{1}{9}A_1^{20}\right) \tag{2A}$$

$$-\frac{9P_1(\cos\theta)}{2k^2}\left[\frac{\cos\alpha_1}{S^2} - \frac{\cos\beta_1}{C^2}\right]\left(\frac{1}{9}\sin\delta_1^{00}\cos\delta_1^{00} + \frac{1}{3}\sin\delta_1^{1\pm}\cos\delta_1^{1\pm} + \frac{1}{6}B_1^{2\pm} + \frac{1}{9}B_1^{20}\right)$$

where

$$\alpha_1 = a \ln S^2 + 2(\sigma_1 - \sigma_0)$$

$$\beta_1 = a \ln C^2 + 2(\sigma_1 - \sigma_0)$$

$$S^2 = \sin^2 \theta/2$$

$$C^2 = \cos^2 \theta/2$$

$$A_\ell^{Jm_s} = \mathrm{Re}(e^{2i\delta_\ell^{Jm_s}} - 1)$$

$$B_\ell^{Jm_s} = \mathrm{Im}(e^{2i\delta_\ell^{Jm_s}})$$

(2A) reduces to the expression given by G. Breit, C. Kittel, and H. M. Thaxton, Physical Review 57, 255, (1940) when the coupling between the $^3P_2$ and $^3F_2$ scattering is neglected.

TABLE I

Singlet phase shifts at 32 Mev for various radial forms adjusted to fit the low energy scattering.

Model	V_c	R	Phase Shift S	Phase Shift D
$V_c(\frac{r}{R}) = \begin{cases} V_c & r < R \\ 0 & r > R \end{cases}$	13.273 Mev	2.615×10^{-13} cm	41.99°	.770°
$V_c(\frac{r}{R}) = V_c e^{-r/R}$	108.27 Mev	$.7088 \times 10^{-13}$ cm	47.54°	1.20°
$V_c(\frac{r}{R}) = \frac{V_c e^{-r/R}}{r/R}$	49.350 Mev	1.1417×10^{-13} cm	51.15°	1.40°

REFERENCES

1. W. K. H. Panofsky and F. Fillmore, UCRL 481

2. C. Richman, B. Cork, and L. Johnston, UCRL 482

3. O. Chamberlain and C. Wiegand, UCRL 553

4. J. Hadley, E. L. Kelly, C. E. Leith, E. Segrè, and H. F. York, Phys. Rev. 75, 351 (1949)

5. K. Brueckner, W. Hartsough, E. Hayward and W. M. Powell, Phys. Rev. 75, 555 (1949)

6. R. S. Christian and E. W. Hart, Phys. Rev. (in press)

7. E. Segrè (private communication)

8. F. L. Yost, J. A. Wheeler, and G. Breit, Phys. Rev. 49, 174 (1936)

   G. Breit, E. U. Condon, and R. D. Present, Phys. Rev. 50, 825 (1936)

   G. Breit, H. M. Thaxton, and L. Eisenbud, Phys. Rev. 55, 1018 (1939)

   L. E. Hoisington, S. S. Share, and G. Breit, Phys. Rev. 56, 884 (1939)

   H. M. Thaxton and L. E. Hoisington, Phys. Rev. 56, 1194 (1939)

9. J. Schwinger, Phys. Rev. 72, 742A (1947)

   J. M. Blatt and J. D. Jackson, Phys. Rev. 76, 18 (1949); also Phys. Rev. (in press)

   H. A. Bethe, Phys. Rev. 76, 38 (1949)

10. G. F. Chew and M. L. Goldberger, Phys. Rev. 75, 1637 (1949)

FIGURE CAPTIONS

Figure 1. Comparison of n-p and p-p scattering data.

Figure 2. Effects of S, D, and P waves on 32 Mev scattering. The upper set of curves give the nuclear scattering. The lower set include the effects of coulomb forces.

Figure 3. Tensor scattering from a singular potential at various energies. The energies in Mev are given parametrically on the curves.

Figure 4. Effect of adding tensor scattering to the singlet scattering at 32 Mev. A. Nuclear scattering. B. Scattering including the effects of coulomb forces. The tensor scattering is that from a potential of exponential radial dependence ($R = .71 \times 10^{-13}$ cm, $V_t = \pm 50$ Mev).

Figure 5. Singlet scattering at 350 Mev as predicted for a potential having Yukawa radial dependence.

Figure 6. Comparison of exact and Born calculations for tensor force scattering at 32 Mev from a potential of Yukawa radial dependence ($R = 1.25 \times 10^{-13}$cm).

Figure 7. Comparison of exact and Born calculations for tensor force scattering at 350 Mev from a potential of Yukawa radial dependence ($R = 1.25 \times 10^{-13}$ cm).

Figure 8. Singlet scattering at 32 Mev from potentials with various radial forms adjusted to fit the low energy scattering. Data taken from reference 2 (31.8 Mev).

Figure 9. P wave scattering added to the singlet scattering predicted by the Yukawa potential at 32 Mev.

Figure 10. Total scattering at 32 Mev by singlet and triplet tensor potentials of the same radial form. (The singlet potentials have range and depth adjusted to fit the low energy scattering.) A. Square B. Exponential C. Yukawa

Figure 11. Singlet plus triplet tensor scattering at 32 Mev. The singlet potential is a square well ($R = 2.615 \times 10^{-13}$ cm, $V_c = 13.273$ Mev), and the tensor potential is a Yukawa potential ($R = 1.25 \times 10^{-13}$ cm, $V_t = \pm 26$ Mev). The experimental points are taken from reference (1) (at 29.4 Mev) and have been reduced in magnitude by 5 percent.

Figure 12. Born tensor scattering amplitude for various potentials. The abscissa scale has been adjusted so that all potentials will give the same angular distribution at 32 Mev as the Yukawa potential with $R = 1.25 \times 10^{-13}$ cm for a suitable choice of depth.

Figure 13. Complete cross section at 350 Mev for various tensor models adjusted to fit the 32 Mev data. The legend shows the tensor model used. Data taken from reference (3).

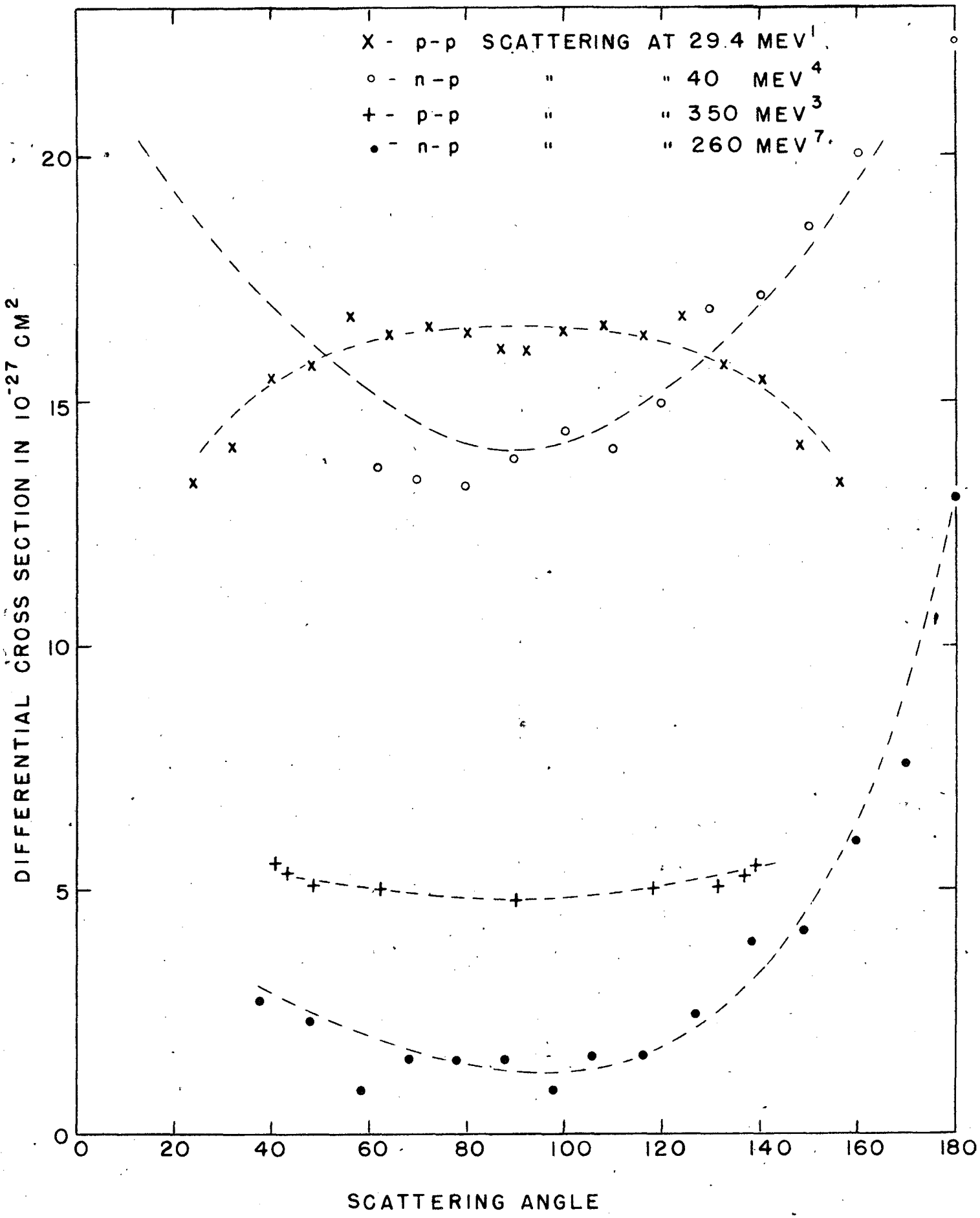
X - p-p SCATTERING AT 29.4 MEV[1]
○ - n-p " " 40 MEV[4]
+ - p-p " " 350 MEV[3]
● - n-p " " 260 MEV[7]
DIFFERENTIAL CROSS SECTION IN 10^{-27} CM^2
SCATTERING ANGLE
0
5
10
15
20
0
20
40
60
80
100
120
140
160
180

FIG. 1

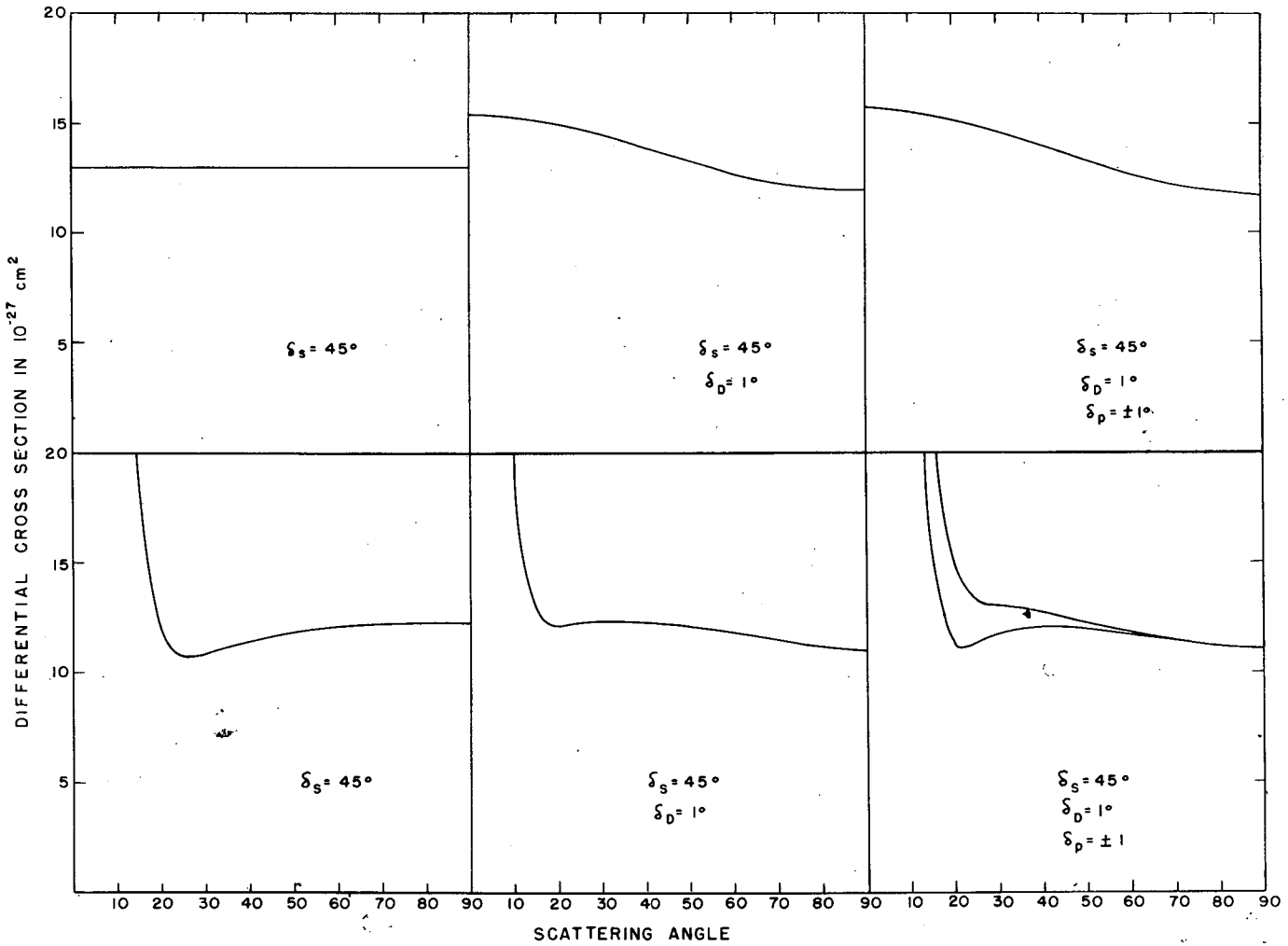
DIFFERENTIAL CROSS SECTION IN 10^{-27} cm^2
SCATTERING ANGLE
$\delta_s = 45°$
$\delta_s = 45°$
$\delta_D = 1°$
$\delta_s = 45°$
$\delta_D = 1°$
$\delta_p = \pm 1°$
$\delta_s = 45°$
$\delta_s = 45°$
$\delta_D = 1°$
$\delta_s = 45°$
$\delta_D = 1°$
$\delta_p = \pm 1$

FIG. 2

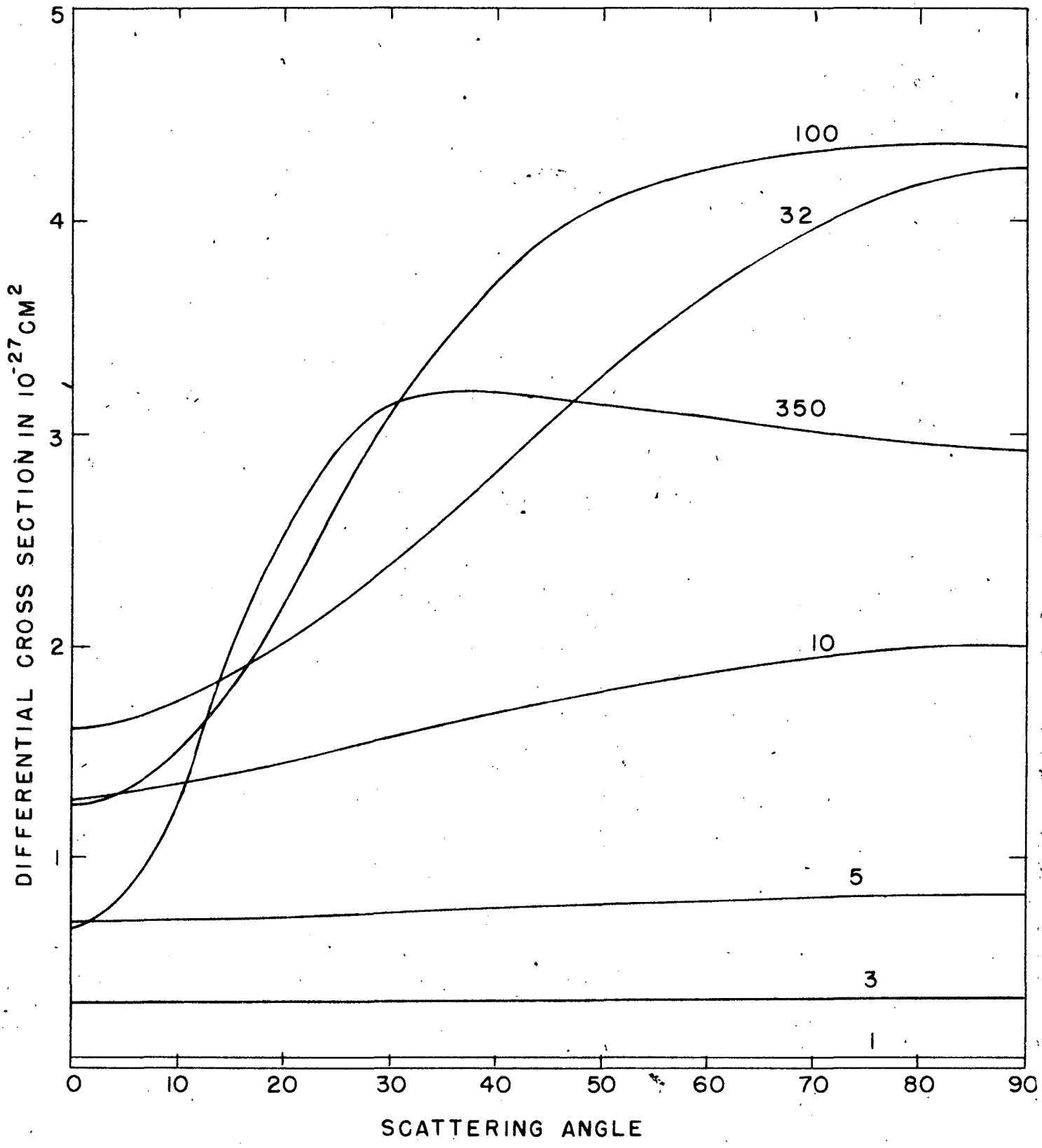
DIFFERENTIAL CROSS SECTION IN 10^{-27} CM^2
5
4
3
2
1
100
32
350
10
5
3
1
0
10
20
30
40
50
60
70
80
90
SCATTERING ANGLE

FIG. 3

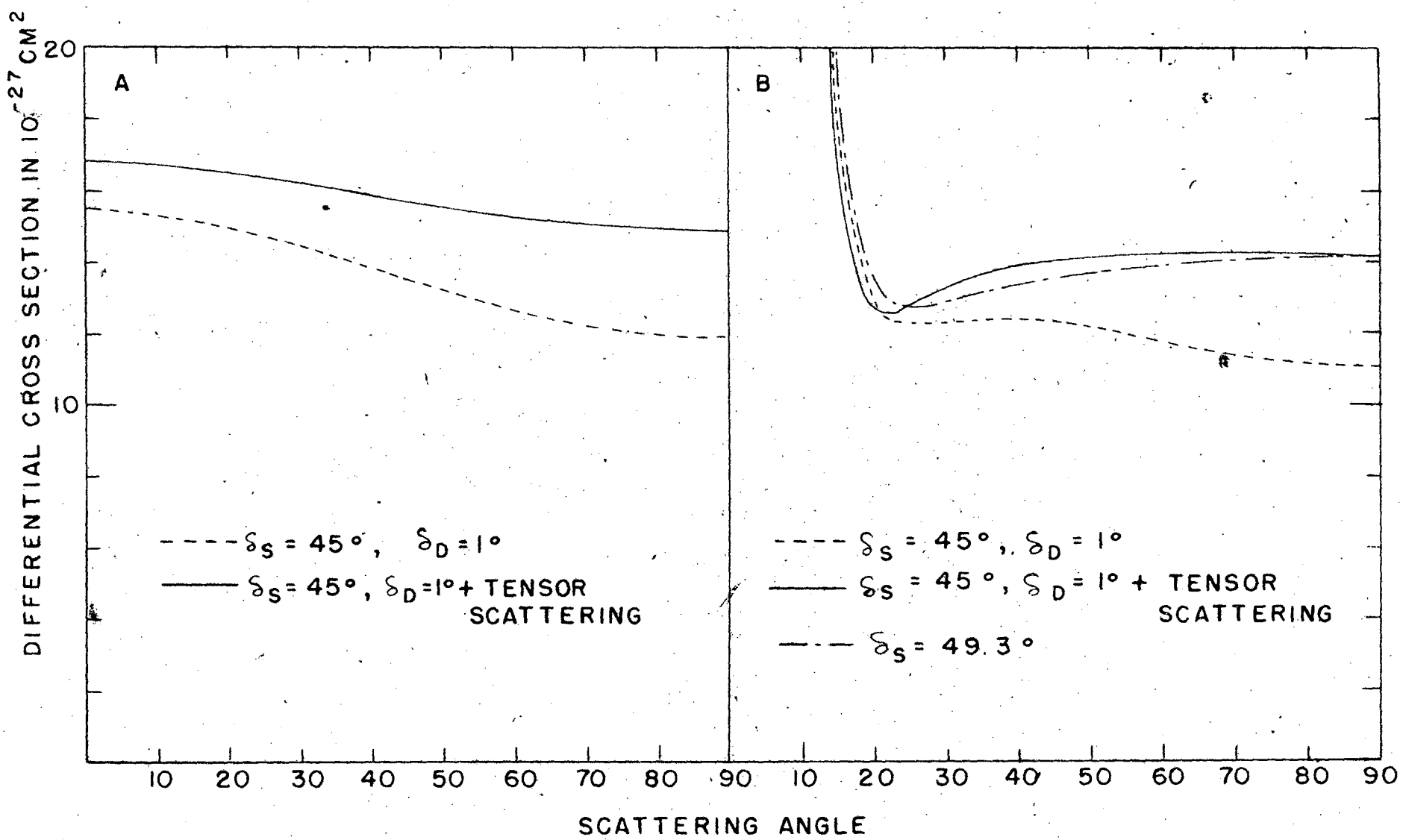
DIFFERENTIAL CROSS SECTION IN 10^{-27} CM^2
20
10
A
B
$\delta_S = 45°$, $\delta_D = 1°$
$\delta_S = 45°$, $\delta_D = 1°$ + TENSOR SCATTERING
$\delta_S = 45°$, $\delta_D = 1°$
$\delta_S = 45°$, $\delta_D = 1°$ + TENSOR SCATTERING
$\delta_S = 49.3°$
10 20 30 40 50 60 70 80 90 10 20 30 40 50 60 70 80 90
SCATTERING ANGLE

FIG. 4

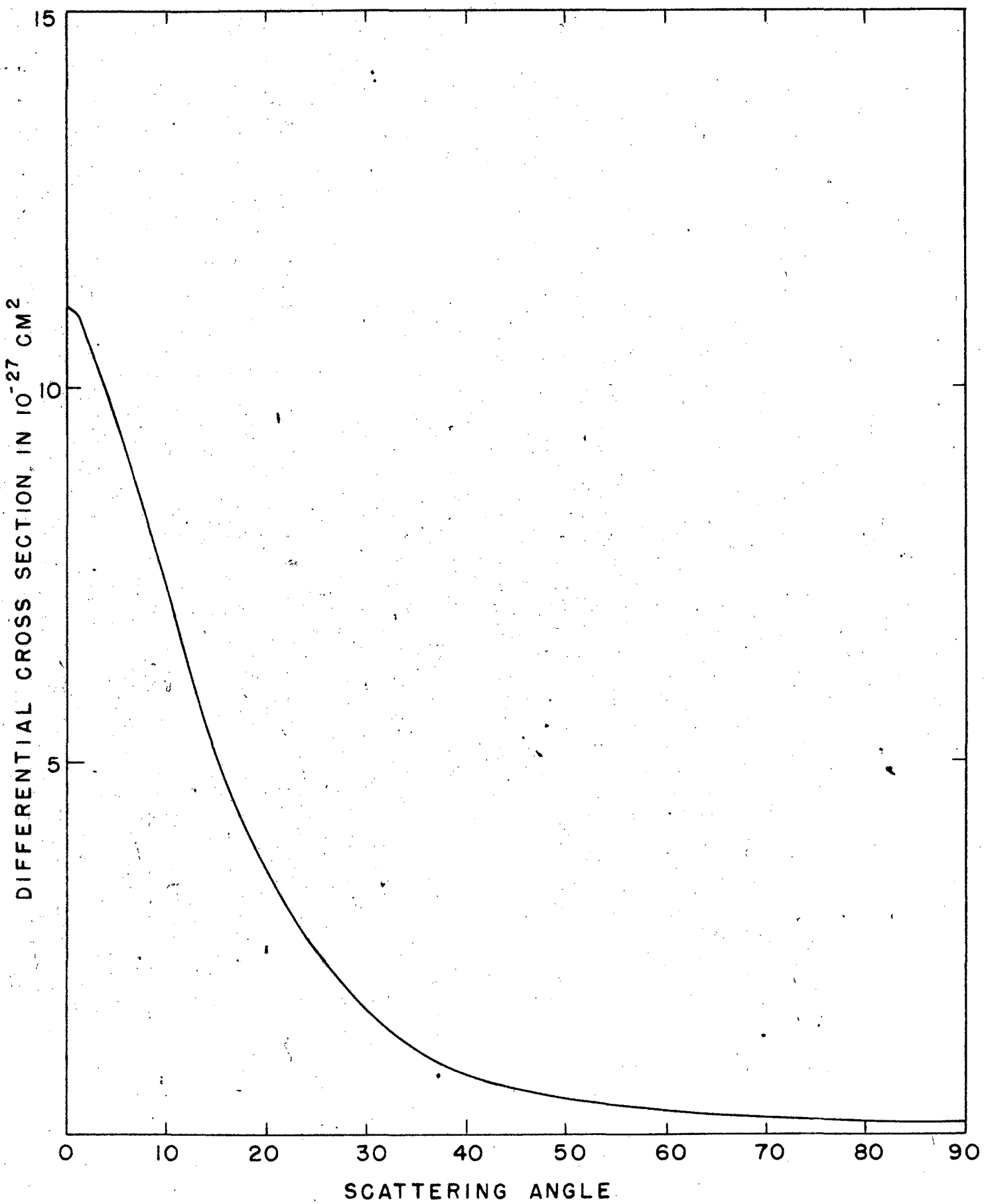
15
10
5
DIFFERENTIAL CROSS SECTION IN 10^{-27} CM^2
0
10
20
30
40
50
60
70
80
90
SCATTERING ANGLE

FIG. 5

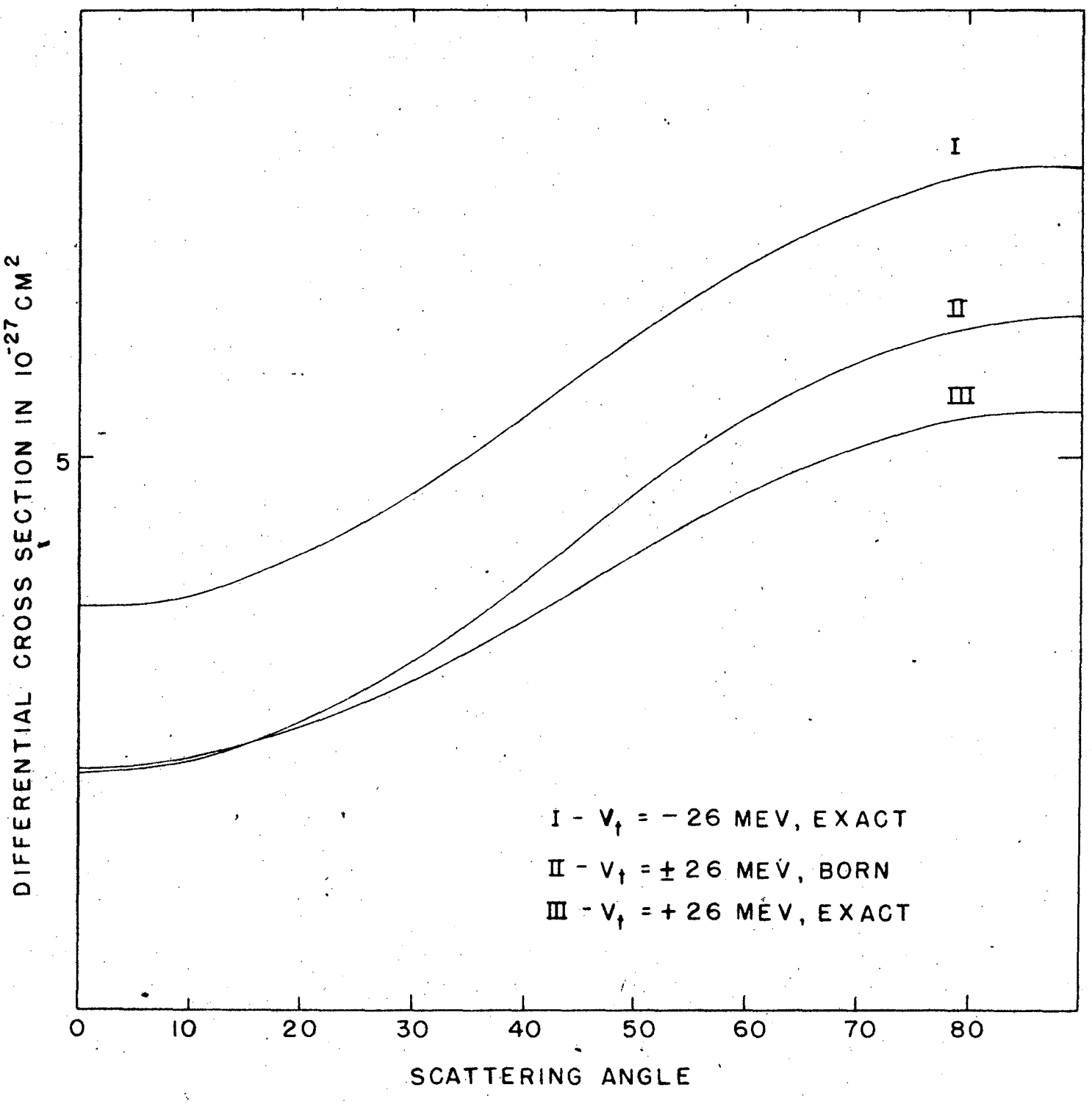
DIFFERENTIAL CROSS SECTION IN 10^{-27} CM^2
5
I
II
III
I - V_t = − 26 MEV, EXACT
II - V_t = ± 26 MEV, BORN
III - V_t = + 26 MEV, EXACT
0
10
20
30
40
50
60
70
80
SCATTERING ANGLE

FIG. 6

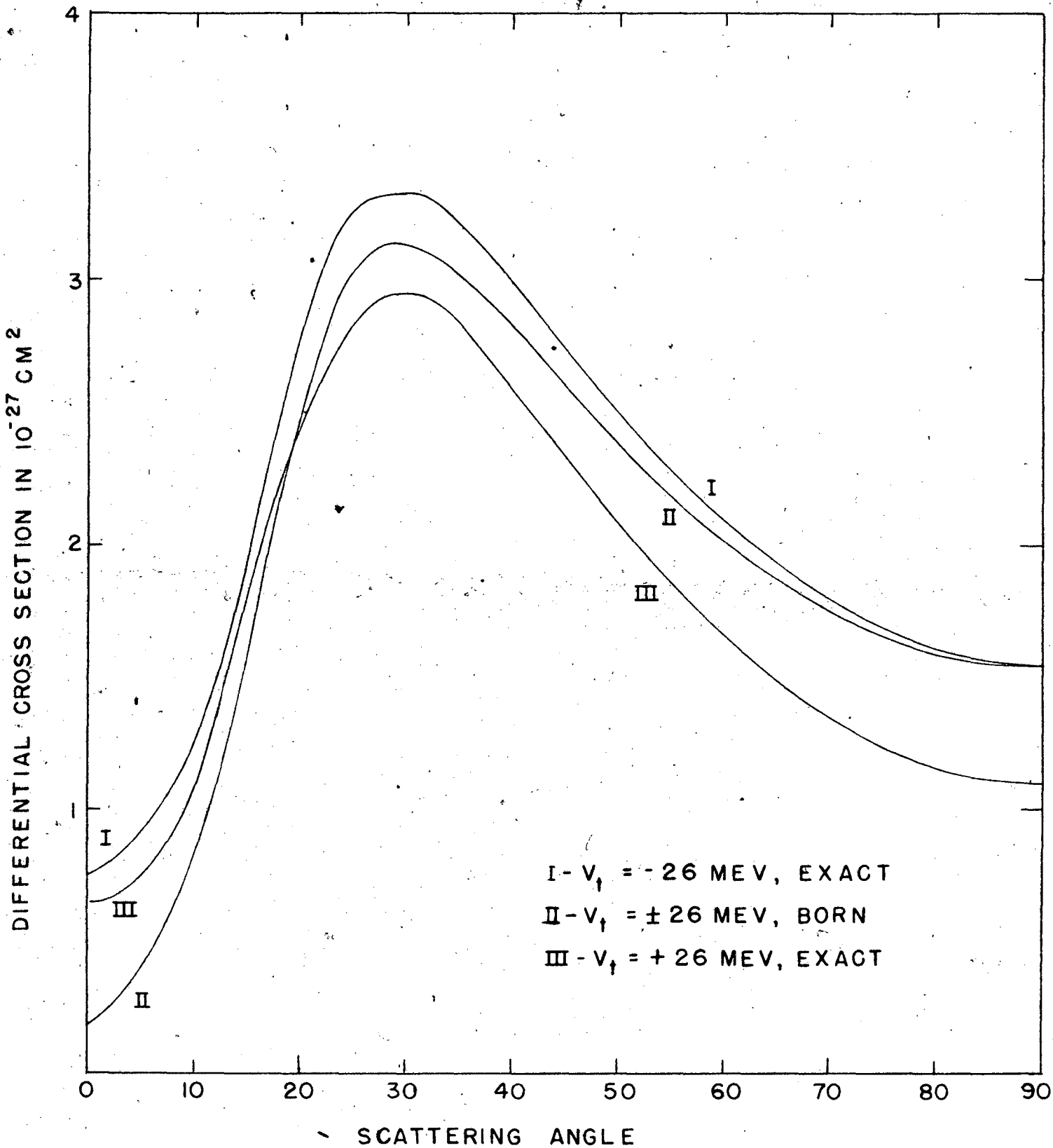
DIFFERENTIAL CROSS SECTION IN 10^{-27} CM^2
SCATTERING ANGLE
0
10
20
30
40
50
60
70
80
90
1
2
3
4
I
II
III
I - V_t = - 26 MEV, EXACT
II - V_t = ± 26 MEV, BORN
III - V_t = + 26 MEV, EXACT

FIG. 7

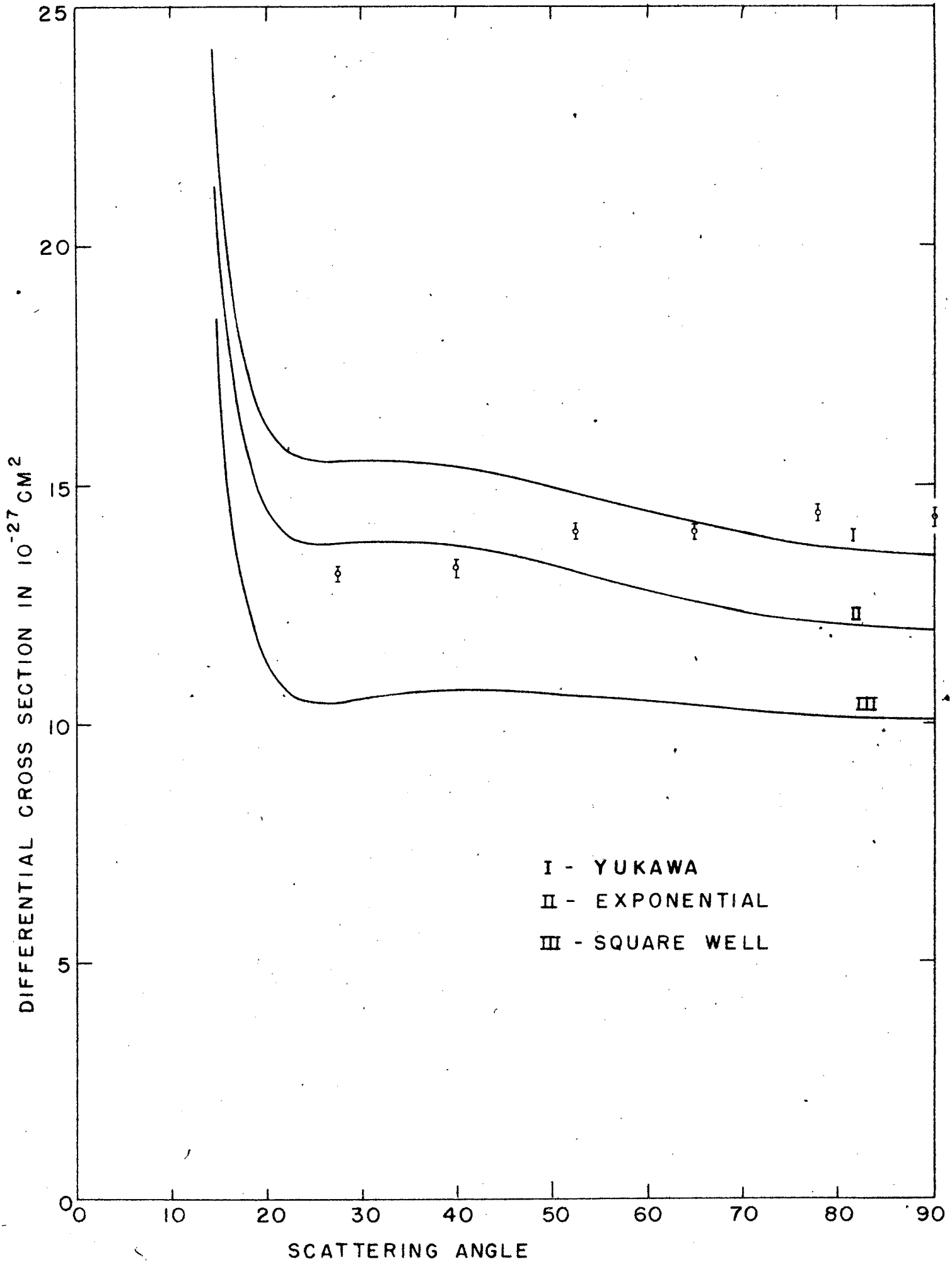
DIFFERENTIAL CROSS SECTION IN 10^{-27} CM^2
SCATTERING ANGLE
0
5
10
15
20
25
0
10
20
30
40
50
60
70
80
90
I
II
III
I - YUKAWA
II - EXPONENTIAL
III - SQUARE WELL

FIG. 8

14395-1

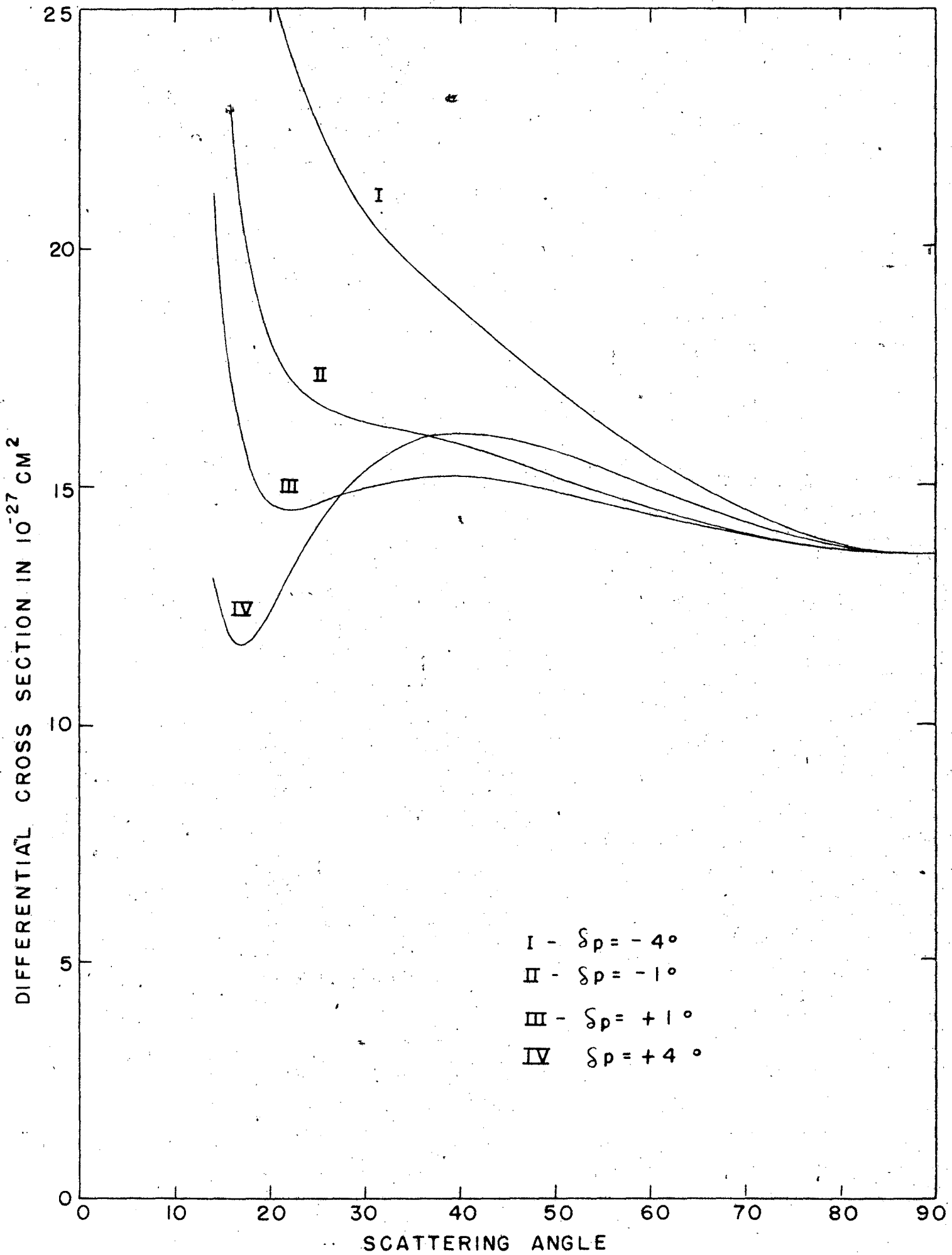
25
20
15
10
5
0
0
10
20
30
40
50
60
70
80
90
DIFFERENTIAL CROSS SECTION IN 10^{-27} CM^2
SCATTERING ANGLE
I
II
III
IV
I - $\delta p = -4°$
II - $\delta p = -1°$
III - $\delta p = +1°$
IV $\delta p = +4°$

FIG. 9

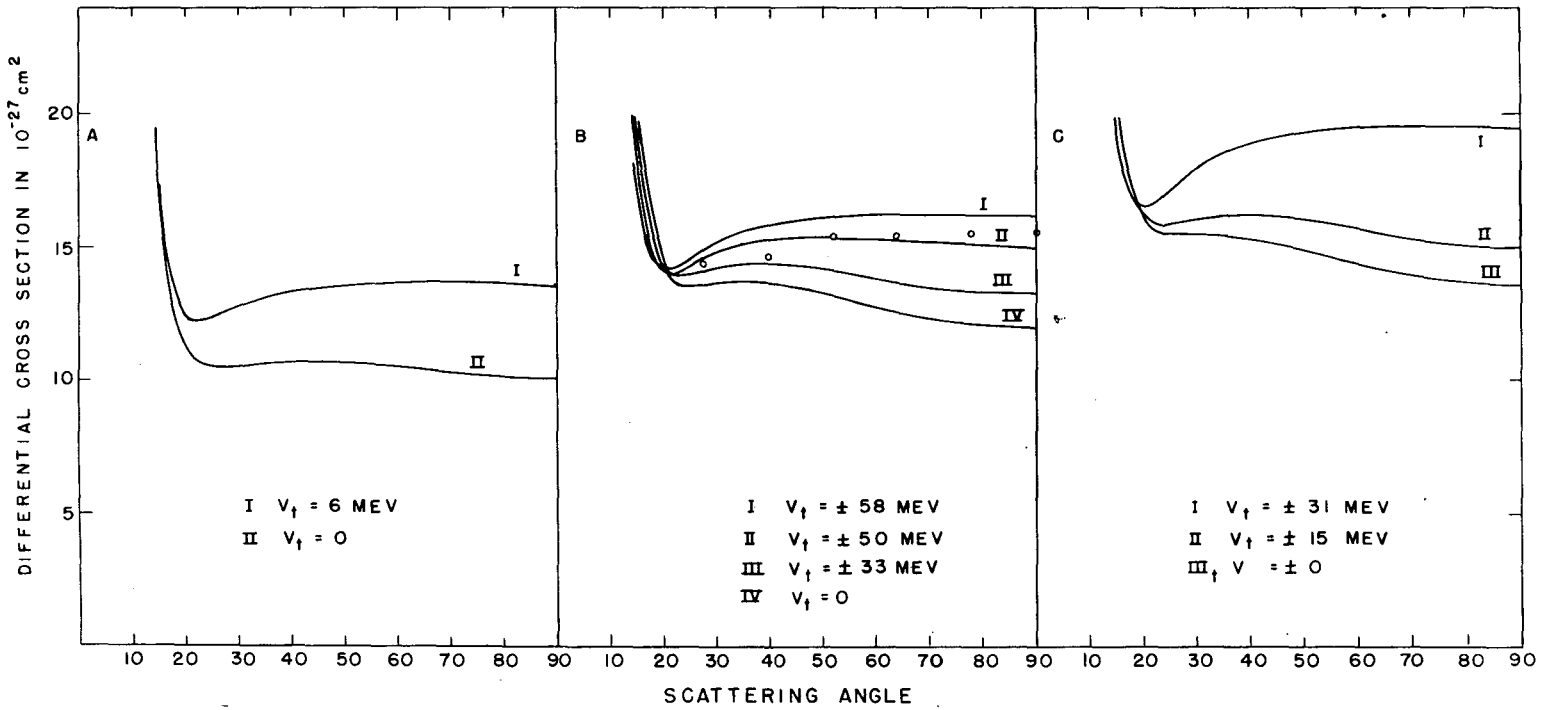
DIFFERENTIAL CROSS SECTION IN 10^{-27} cm^2
20
15
10
5
A
I
II
I V_t = 6 MEV
II V_t = 0
B
I
II
III
IV
I V_t = ± 58 MEV
II V_t = ± 50 MEV
III V_t = ± 33 MEV
IV V_t = 0
C
I
II
III
I V_t = ± 31 MEV
II V_t = ± 15 MEV
III V_t = ± 0
10 20 30 40 50 60 70 80 90
SCATTERING ANGLE

FIG. 10

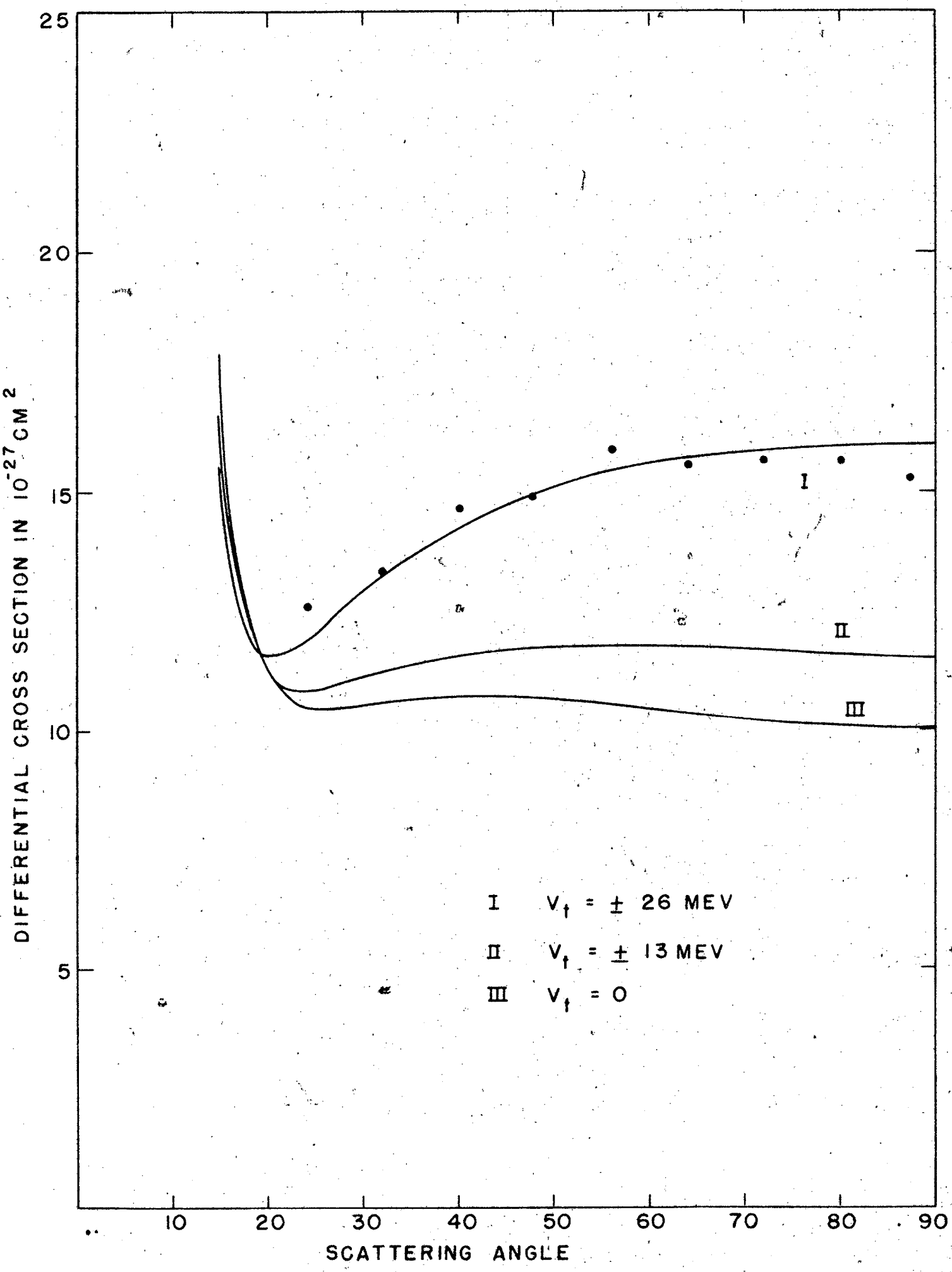
25
20
15
10
5
DIFFERENTIAL CROSS SECTION IN 10^{-27} CM^2
10
20
30
40
50
60
70
80
90
SCATTERING ANGLE
I
II
III
I $V_f = \pm$ 26 MEV
II $V_f = \pm$ 13 MEV
III $V_f = 0$

FIG. 11

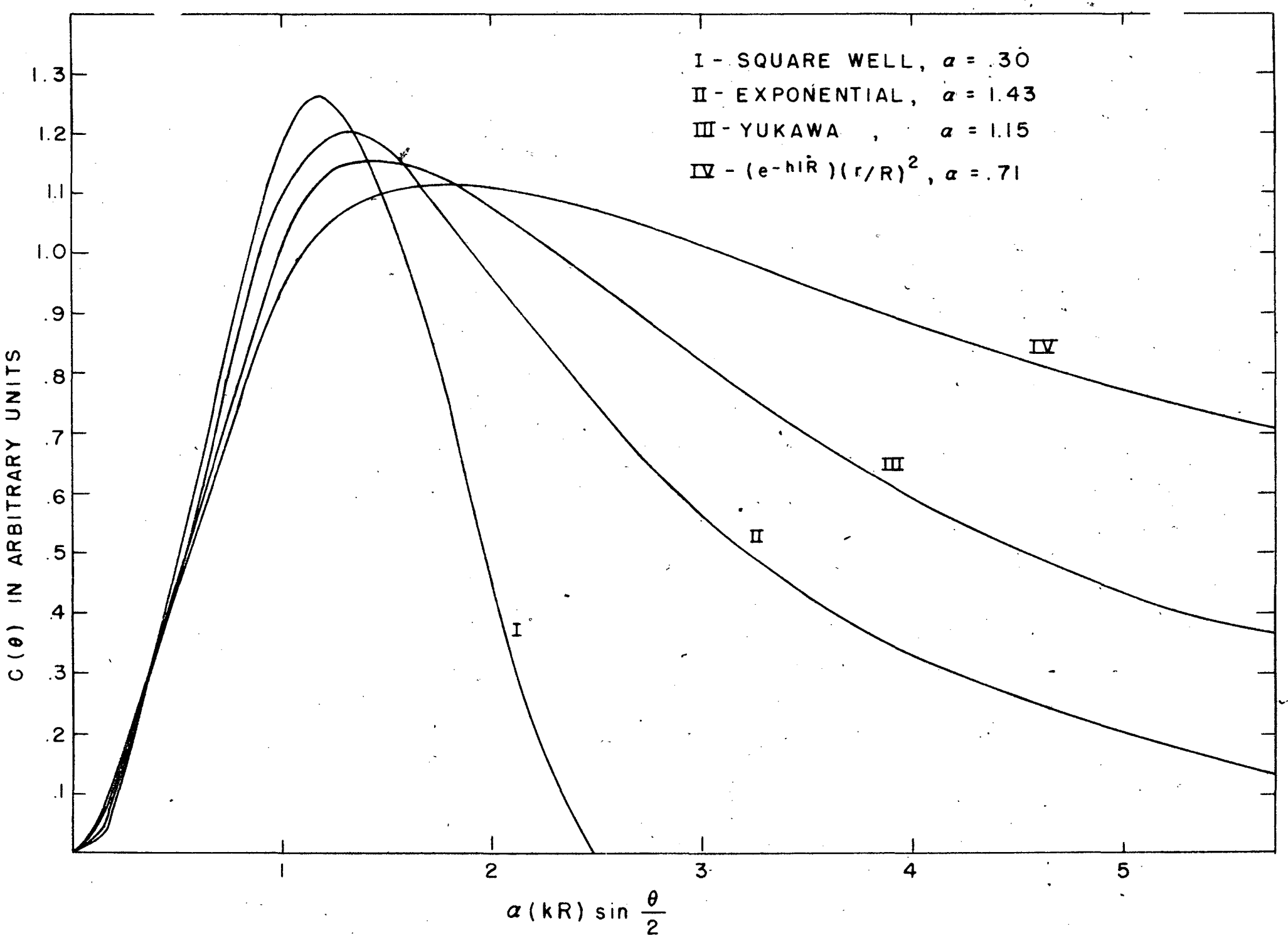
I - SQUARE WELL, α = .30
II - EXPONENTIAL, α = 1.43
III - YUKAWA , α = 1.15
IV - (e^{-hR})(r/R)^2, α = .71
C(θ) IN ARBITRARY UNITS
1.3
1.2
1.1
1.0
.9
.8
.7
.6
.5
.4
.3
.2
.1
1
2
3
4
5
α(kR) sin θ/2
I
II
III
IV

FIG. 12

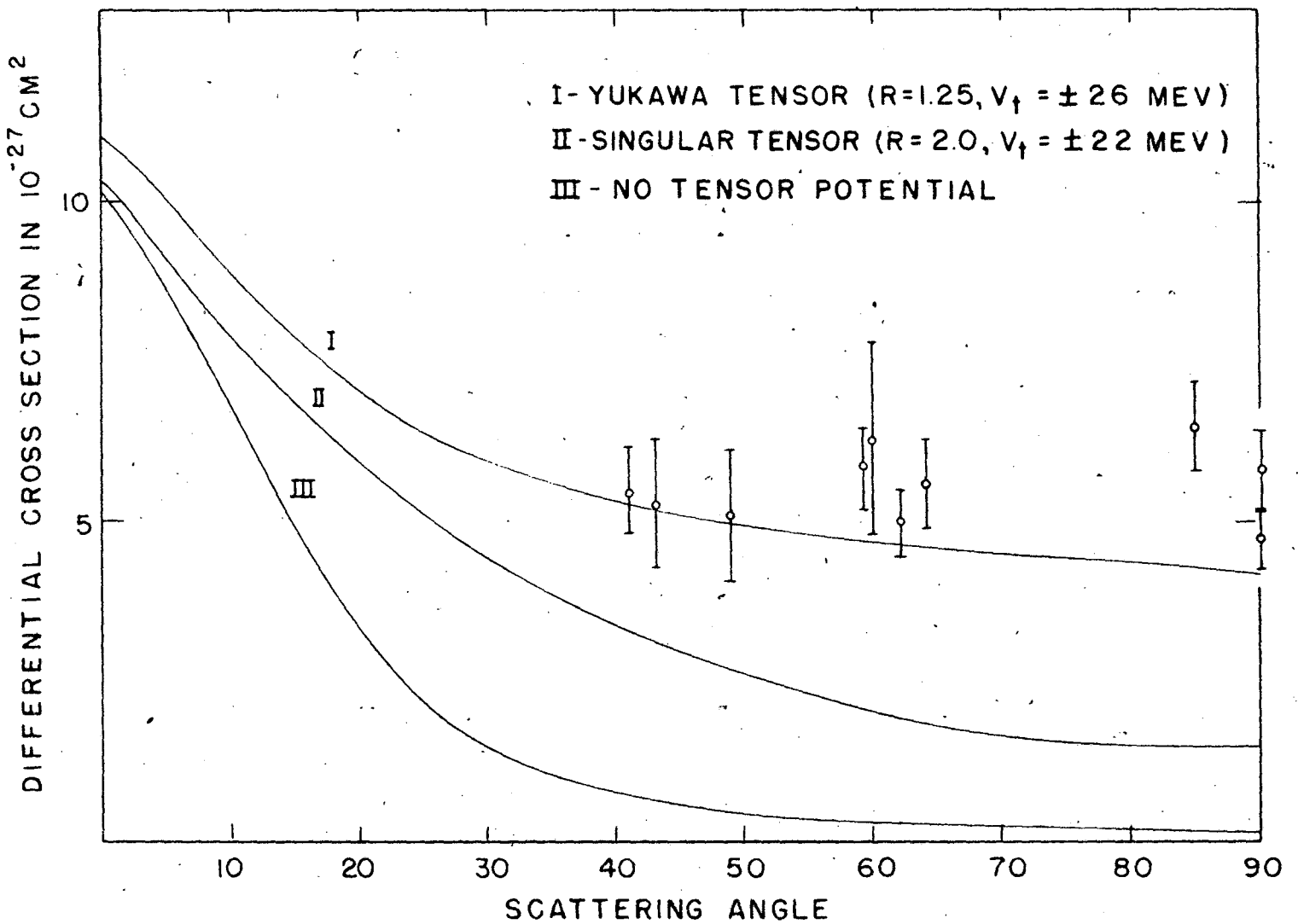
I- YUKAWA TENSOR (R=1.25, V_t = ± 26 MEV)
II-SINGULAR TENSOR (R= 2.0, V_t = ± 22 MEV)
III - NO TENSOR POTENTIAL
I
II
III
10
5
DIFFERENTIAL CROSS SECTION IN 10^{-27} CM^2
10
20
30
40
50
60
70
80
90
SCATTERING ANGLE

FIG. 13